The Astrophysical Journal, 977:121 (5pp), 2024 December 10 https://doi.org/10.3847/1538-4357/ad93a3

Exploring Magnetic Fields in a Merging Galaxy: Comparing Polarization and Velocity Gradient in the Centaurus Galaxy

Quynh Lan Nguyen[1,2], Yue Hu[3,5], and Alex Lazarian[4]
[1] Phenikaa Institute for Advanced Study, Phenikaa University, Yen Nghia, Ha Dong, Hanoi 100000, Vietnam; lan.nguyenquynh@phenikaa-uni.edu.vn
[2] Department of Physics and Astronomy, University of Notre Dame, Notre Dame, IN 46556, USA
[3] Institute for Advanced Study, 1 Einstein Drive, Princeton, NJ 08540, USA; yuehu@ias.edu
[4] Department of Astronomy, University of Wisconsin-Madison, Madison, WI 53706, USA; lazarian@astro.wisc.edu
Received 2024 June 5; revised 2024 October 30; accepted 2024 November 15; published 2024 December 9

Abstract

In this study, we apply the velocity gradient technique to the merging Centaurus galaxy. We compare gradient maps derived from the PHANGS-Atacama Large Millimeter/submillimeter Array survey using CO emission lines with magnetic field tracings from dust polarization data obtained via the HAWC+ instrument. Our analysis reveals a strong correspondence between the directions indicated by these two tracers across most of the galactic image. Specifically, we identify jet regions as areas of antialignment, consistent with previous reports that gradients tend to rotate 90° in outflow regions. Statistically, we find that the alignment of magnetic fields, as revealed by polarization, is most accurate in regions with the highest signal-to-noise ratios. Our findings underscore the utility of velocity gradients as a valuable complementary tool for probing magnetic fields and dynamical processes in merging galaxies. This proves the general utility of velocity gradients for mapping magnetic fields in astrophysical objects with complex dynamics.

Unified Astronomy Thesaurus concepts: Extragalactic magnetic fields (507); Interstellar medium (847); Galaxy nuclei (609)

1. Introduction

Merging plays an important role in the galaxy's evolution, so tracing the magnetic field in the merging galaxy is interesting. It can provide valuable insight into the dynamic and evolution of the galaxy, as well as the jet formation (J. Whittingham et al. 2021). Through the interaction of the magnetic field in the merging galaxy and the magnetic field in the interstellar medium and other galaxies and cluster galaxies, we can better understand the formation and shape of the large-scale structure of the Universe (K. Rodenbeck & D. R. G. Schleicher 2016; V. S. Paliya et al. 2020; J. O. Chibueze et al. 2021).

The observations in the far-infrared and radio for galactic and extragalactic magnetic fields have developed significantly in the past decades (P. P. Kronberg 1994; R. Beck 2015; E. Lopez-Rodriguez 2021). Even if it has some initial results, it still has some limitations. Dust and synchrotron polarization can trace the plane-of-the-sky (POS) magnetic field orientation. However, dust polarization is affected by dust alignment efficiency (A. Lazarian & T. Hoang 2007), and synchrotron polarization is subject to Faraday rotation (R. Beck 2015). Synchrotron polarization provides the method that can trace the magnetic fields in the warm and high temperatures of the gas (R. Beck 2001; A. Fletcher et al. 2011; R. Beck 2015) and dust polarization contains contributions from different gas phases, including the one associated with diffuse atomic gas and dense molecular gas (A. Lazarian & T. Hoang 2007; B. G. Andersson et al. 2015).

To separate the magnetic field associated with molecular gas, which is the most important fueling material for the galactic nuclei, Y. Hu et al. (2022) proposed the use of the velocity gradient technique (VGT; D. F. González-Casanova & A. Lazarian 2017; A. Lazarian & K. H. Yuen 2018; Y. Hu et al. 2018) and CO spectroscopic observations. Despite that, the study of VGT has been explored for seven individual galaxies: M51, NGC 1068, NGC 1097, NGC 3627, NGC 4826 (Y. Hu et al. 2022), NGC 3627 (M. Liu et al. 2023), and NGC 0628 (M. Zhao et al. 2024), but its application or test to galaxy merger has not yet been done. Centaurus galaxy, as one of the closest nuclear active galaxy mergers, is the best test-bed for VGT.

In this work, we trace the magnetic field of the Centaurus galaxy using the VGT, particularly its branch, namely, velocity channel gradients (A. Lazarian & K. H. Yuen 2018) and ^{12}CO ($J = 2$–1) emission lines from the Physics at High Angular Resolution in Nearby Galaxies-Atacama Large Millimeter/submillimeter Array (PHANGS-ALMA) survey (A. K. Leroy et al. 2021). On the other hand, the magnetic field in Centaurus has been studied by (E. Lopez-Rodriguez 2021) using High-resolution Airborne Wideband Camera Plus (HAWC+) dust polarization at 89 μm. Here we compare the magnetic field traced by VGT to the one inferred from HAWC+.

However, it should be noted that the dynamics of galaxy mergers are more complicated than normal galaxies. This makes the interpretation of the comparison more difficult. For instance, early applications by Y. Hu et al. (2022), M. Liu et al. (2023), and M. Zhao et al. (2024) of the VGT have conventionally set the turbulence injection scale, $L_{\rm inj}$, at approximately 100 pc, a measure derived from extensive studies of turbulence within the Milky Way (J. W. Armstrong et al. 1995; A. Chepurnov & A. Lazarian 2010; T. Ha et al. 2022). This assumption aligns with the typical scale at which energy is injected into the interstellar medium via stellar

[5] NASA Hubble Fellow.

feedback and other dynamic processes in relatively stable galactic environments. However, in scenarios involving galaxy mergers, the dynamics of turbulence injection can be substantially altered. Mergers not only impact galactic structure and star formation but also contribute to turbulence on a much larger scale (J. Whittingham et al. 2021). The merging process itself can act as a significant driver of turbulence, likely extending the injection scale well beyond the 100 pc typically observed in more quiescent galaxies like the Milky Way. Given this context, it is reasonable to hypothesize that the injection scale $L_{\rm inj}$ in the Centaurus galaxy, which has experienced dynamic merger events, could be larger than 100 pc and we expect the ^{12}CO observation with an average spatial resolution of 145.5 pc to satisfy the VGT's requirements for this pilot study.

The details of the archival data are shown in Section 2. Centaurus galaxy is one of the closest nuclear active galaxies and we want to use it as a test for VGT. In Section 3, we introduce the detailed theory of the VGT, velocity caustics, and VGT pipeline. In Section 4, we will discuss some results about the mapping magnetic field of the Centaurus galaxy and compare it with dust polarization result. In Section 5, we will provide some conclusions about the magnetic fields of the Centaurus galaxy using VGT.

2. Observational Data

2.1. Emission Lines

In this study, we utilized the ^{12}CO ($J = 2$–1) emission lines provided by the PHANGS-ALMA survey (A. K. Leroy et al. 2021). The PHANGS-ALMA survey offers ^{12}CO ($J = 1$–0) emission line data at a spatial resolution of approximately $8\farcs13$ (about 145.5 pc) and a velocity resolution of 2.5 km s^{-1} for the nearby galaxy Centaurus. This survey achieves a high signal-to-noise ratio, with an rms brightness temperature noise level around $\sim 0.30 \pm 0.13$ K km s^{-1}.

2.2. Polarization Measurement

For polarization measurements, we employed data from the HAWC+ archived in the HAWC+ database (D. A. Harper et al. 2018; E. Lopez-Rodriguez 2021). Magnetic field orientations were determined using the relation $\phi_B = \phi + \pi/2$, where ϕ represents the polarization angle. Measurements were taken from band C (89 μm, FWHM $\approx 7\farcs8$).

We limited our analysis to pixels where the polarization fraction (p) divided by its uncertainty (σ_p) exceeds 1 ($p/\sigma_p > 1$). To compare with the magnetic field measured with VGT, we smooth the polarization data to FWHM $\approx 40''$ matching the spatial resolution of VGT.

3. Methodology

3.1. Theoretical Consideration: VGT

The theoretical underpinning of the VGT lies in the anisotropy inherent in MHD turbulence, a concept extensively developed by P. Goldreich & S. Sridhar (1995) and A. Lazarian & E. T. Vishniac (1999). This anisotropy suggests that turbulent eddies elongate along magnetic field lines, manifesting notably in local reference frames. A. Lazarian & E. T. Vishniac (1999) formalized this anisotropy as follows:

$$l_{\parallel} = L_{\rm inj}\left(\frac{l_{\perp}}{L_{\rm inj}}\right)^{\frac{2}{3}} M_{\rm A}^{-4/3}, \quad M_{\rm A} \leqslant 1, \tag{1}$$

where $l_{\perp}$ and $l_{\parallel}$ are the scales perpendicular and parallel to the local magnetic field, respectively. Here, $M_{\rm A} = v_{\rm inj}/v_{\rm A}$ represents the Alfvén Mach number, with $v_{\rm inj}$ being the injection velocity and $v_{\rm A}$ the Alfvén speed.

This anisotropy has been demonstrated by numerical simulations (J. Cho & E. T. Vishniac 2000; J. Maron & P. Goldreich 2001; J. Cho & A. Lazarian 2003; G. Kowal & A. Lazarian 2010; Y. Hu et al. 2021) and in situ measurements in the solar wind (X. Wang et al. 2016; L. Matteini et al. 2020; D. Duan et al. 2021; S. Zhao et al. 2024). From Equation (1), we understand that $l_{\parallel}$ significantly exceeds $l_{\perp}$, leading to the dominance of the gradient of velocity fluctuations perpendicular to the local magnetic field:

$$\nabla v_l \approx \frac{v_{l,\perp}}{l_{\perp}} = \frac{v_{\rm inj}}{L_{\rm inj}} M_{\rm A}^{1/3}\left(\frac{l_{\perp}}{L_{\rm inj}}\right)^{-2/3}, M_{\rm A} \leqslant 1. \tag{2}$$

This scaling relation ($\propto l_{\perp}^{-2/3}$) is crucial as it reveals that the amplitude of the turbulent velocity gradient increases at smaller scales, which is a characteristic not typically observed in nonturbulent velocity fields such as galactic differential rotation. For effective application to external galaxies, observations should resolve the scale at which turbulence's anisotropy manifests prominently, typically at $L_{\rm inj}$ for sub-Alfvén and trans-Alfvén turbulence or $L_{\rm inj} M_{\rm A}^{-3}$ for super-Alfvénic turbulence (A. Lazarian 2006).

3.2. Velocity Caustics

The anisotropic nature of MHD turbulence can be observed in velocity channel maps, $p(x, y, v_{\rm los})$, obtained from spectroscopic observations. This observation is primarily due to the velocity caustics effect, which posits that real density structures with different velocities may be sampled into the same velocity channel, thereby significantly altering the observed intensity structures within the spectroscopic channel maps (A. Lazarian & D. Pogosyan 2000, 2004; D. Kandel et al. 2016; Y. Hu et al. 2023).

Mathematically, the intensity observed in a channel can be expressed as the sum of two terms (Y. Hu et al. 2023):

$$p(x, y, v_{\rm los}) = p_v(x, y, v_{\rm los}) + p_d(x, y, v_{\rm los}), \tag{3}$$

where p_v represents fluctuations primarily caused by velocity—known as the velocity caustics effect—while p_{dc} reflects the inhomogeneities within the actual density field. The relative contribution of these terms is dependent on the channel width, i.e., the velocity resolution of the observation. A narrower channel width enhances the contribution of p_v, leading to a scenario where intensity fluctuations in thin channels are predominantly due to velocity fluctuations. Specifically, when the channel width Δv is narrower than the velocity dispersion of the turbulent eddies under observation, the intensity fluctuations within such a thin channel will be primarily driven by velocity fluctuations.

Turbulence studies within the Milky Way suggest that the velocity dispersion at a scale of 100 pc is approximately 10 km s^{-1} (J. W. Armstrong et al. 1995; A. Chepurnov & A. Lazarian 2010; T. Ha et al. 2022). This dispersion can be

even higher in environments such as galaxy mergers. Given that the PHANGS-ALMA survey offers a velocity resolution of 2.5 km s^{-1}, this ensures that the velocity caustics dominate the observed intensity in the spectroscopic velocity channels.

3.3. VGT Pipeline

In this study, we employed the VGT, following a multistep process detailed in (Y. Hu et al. 2022; M. Liu et al. 2023):

Step 1. Each thin channel map, $p(x, y, v_{\rm los})$, undergoes convolution with 3×3 Sobel kernels G_x and G_y to compute the gradients:

$$\nabla_x p(x, y, v_{\rm los}) = G_x * p(x, y, v_{\rm los}),$$
$$\nabla_y p(x, y, v_{\rm los}) = G_y * p(x, y, v_{\rm los}), \quad (4)$$

where $*$ denotes convolution. These gradients are used to determine the pixelized gradient map $\psi_g(x, y, v_{\rm los})$:

$$\psi_g(x, y, v_{\rm los}) = \tan^{-1}\left(\frac{\nabla_y p(x, y, v_{\rm los})}{\nabla_x p(x, y, v_{\rm los})}\right). \quad (5)$$

Only pixels with a brightness temperature less than 3 times the rms noise are retained for subsequent analysis.

Step 2. The pixelized map $\psi_g(x, y, v_{\rm los})$ is segmented into 20×20 pixel sub-blocks—although other sizes have been tested (K. H. Yuen & A. Lazarian 2017; A. Lazarian & K. H. Yuen 2018; Y. Hu et al. 2020a)—and processed as follows:

1. A histogram of gradient orientations within each sub-block is produced and fitted with a Gaussian distribution.
2. The peak of this Gaussian distribution is taken as the dominant gradient orientation for that sub-block.

Step 3. Following sub-block averaging, the averaged gradient angle map $\psi_{gs}(x, y, v_{\rm los})$ is compiled for each velocity channel. Repeating Steps 1 and 2 for every channel within the velocity range of interest, we can then construct the pseudo-Stokes parameters $Q_g(x, y)$ and $U_g(x, y)$:

$$Q_{\rm g}(x, y) = \int_{v_{\rm los,min}}^{v_{\rm los,max}} p(x, y, v_{\rm los}) \cos(2\psi_{gs}(x, y, v_{\rm los}))\, dv_{\rm los},$$
$$U_{\rm g}(x, y) = \int_{v_{\rm los,min}}^{v_{\rm los,max}} p(x, y, v_{\rm los}) \sin(2\psi_{gs}(x, y, v_{\rm los}))\, dv_{\rm los}, \quad (6)$$

where $v_{\rm los,max}$ and $v_{\rm los,min}$ represent the upper and lower levels of the velocity range used for integration. The POS magnetic field orientation is inferred from

$$\psi_{\rm B}(x, y) = \frac{1}{2}\tan^{-1}\left(\frac{U_{\rm g}(x, y)}{Q_{\rm g}(x, y)}\right) + \frac{\pi}{2}. \quad (7)$$

To quantify the agreement between VGT and the magnetic field inferred from polarization, we utilize the alignment measure (AM; D. F. González-Casanova & A. Lazarian 2017), expressed as

$$\mathrm{AM} = 2\left(\cos^2\theta_{\rm r} - \frac{1}{2}\right). \quad (8)$$

Here, $\theta_{\rm r} = |\phi_{\rm B} - \psi_{\rm B}|$, where $\phi_{\rm B}$ is the magnetic field angle inferred from polarization. An AM value of 1 implies parallel alignment of $\phi_{\rm B}$ and $\psi_{\rm B}$, while -1 indicates perpendicularity.

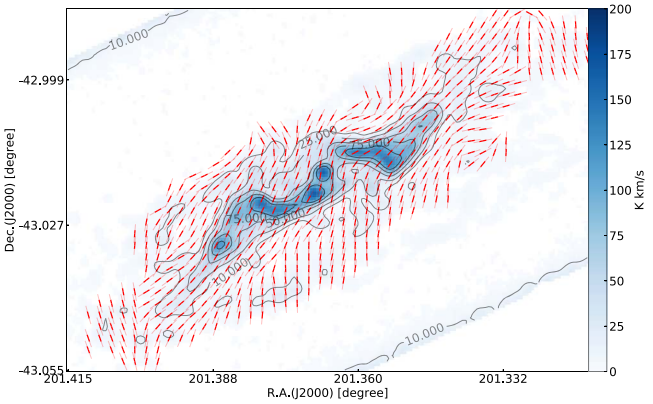

Figure 1. The magnetic field of Centaurus mapped with VGT using the CO (2–1) emission line. The magnetic field segments are laid upon Centaurus' CO emission intensity map.

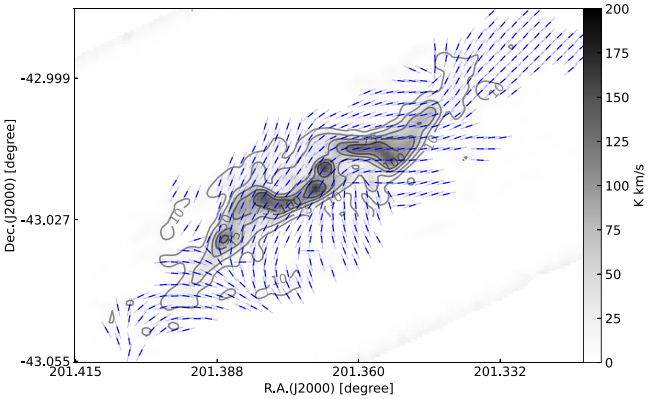

Figure 2. Same as Figure 1, but the magnetic field is measured by HAWC+ polarization at 89 μm.

4. Result

Figure 1 presents the magnetic fields of Centaurus as mapped by VGT-CO. The image captures the twisting of the magnetic field from the southeast and northwest filamentary structures, which resemble spiral-arm-like features, toward the molecular disk and into the nucleus. The magnetic field, as depicted by VGT-CO, primarily aligns with these two filamentary structures. However, it exhibits a twist across the central region of approximately 500 pc radius around the nucleus. Additionally, the magnetic fields inferred from HAWC+ polarization, illustrated in Figure 2, exhibit similar morphology and generally agree with the measurements from VGT-CO. Notably, near the southeast tail, the polarization-inferred magnetic field diverges from the galactic structure indicated by CO, instead crossing it. This specific pattern is absent in the VGT-CO measurements.

The misalignment between the magnetic fields traced by VGT-CO and those indicated by dust polarization is quantified by the AM, as shown in Figure 3. The antialignment, indicated by negative AM values, is observed in the two tails, while a misalignment with AM $\approx$0 is noted in the northwest of the central disk. A higher degree of the mean alignment is observed in several Seyfert galaxies and the Milky Way (Y. Hu et al. 2022; M. Liu et al. 2023; M. Zhao et al. 2024). We attribute this effect to the fact that the Centaurus is a merging galaxy with much more complex dynamics of gas. Jets, shocks, and inflows affect the gradients, especially if the measurements are

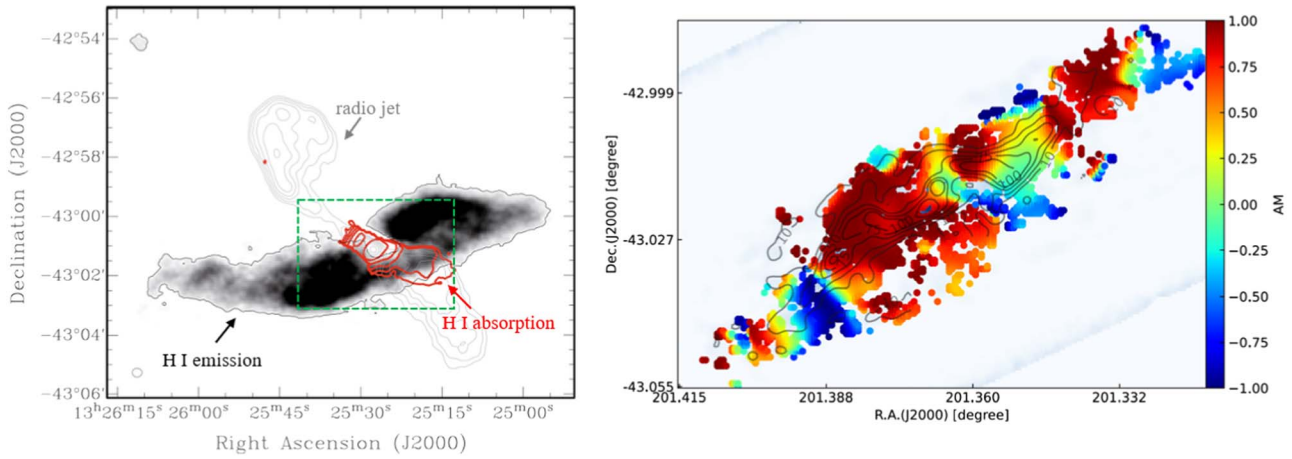

Figure 3. Left: H I emission in grayscale overlaid with radio continuum contours (gray) and H I absorption contours (red). The green box highlights the region where we are studying the VGT-CO. Reproduced with permission ©ESO, C. Struve et al. (2010). Right: the spatial distributions of the AM between VGT-CO measurement and HAWC+ polarization with a resolution of FWHM 40″.

of insufficient resolution. These effects were discussed at length in A. Lazarian & K. H. Yuen (2018), Y. Hu et al. (2019, 2020b), and M. Liu et al. (2024). In particular, antialignment is present in the radio jet regions, which is expected for the outflow regions. Further studies of the origin of this discrepancy are required. This can elucidate the dynamics of gas in the merging galaxy.

Another source of the observed misalignment can be the difference in CO and dust distribution in these regions. Unlike CO, dust is well mixed with all interstellar phases, including molecular and atomic gas (B. G. Andersson et al. 2015). In Figure 3, we see the central low-AM region is associated with strong H I absorption, suggesting the dust polarization in that region might be dominated by dust associated with H I rather than CO. In addition, HAWC+ dust polarization at 89 μm is anticipated to trace magnetic fields in warmer media than CO. If magnetic fields in warm and cold gas are very different, there is a warmer phase preferentially traced by HAWC+; the morphology of magnetic fields with low-AM could reflect that the magnetic fields in warm and cold gas are different.

We also note that the most significant misalignment between VGT-CO and dust polarization measurements is in the low-density regions associated with poor signal-to-noise ratio. This is illustrated in Figure 4, where we observe that we do not observe a negative AM at the high signal-to-noise ratio regions.

Overall, the global agreement between the magnetic field orientations measured with VGT-CO and those inferred from dust polarization, especially in the central disk, underscores the coherence of magnetic fields across different gas phases. This includes the cold molecular phase traced by CO and warmer phases indicated by HAWC+. In places where this coherence is observed, it indicates that across these different interstellar medium phases, the magnetic field thread by the magnetic fields has little effect from density change. Such cases correspond to the notion that molecular clouds correspond to a unified magnetized ecosystem evolving during the merger. Additional input from synchrotron polarization could be useful for getting more information. In the aforementioned studies of Seyfert galaxies with VGT (Y. Hu et al. 2022; M. Liu et al. 2023; M. Zhao et al. 2024), the alignment between the velocity gradients in CO and synchrotron could be better than the alignment with dust, which elucidated the 3D magnetic field structure.

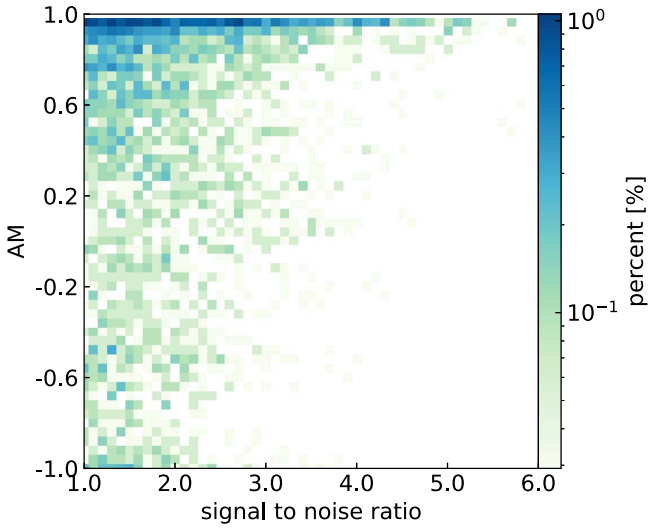

Figure 4. A 2D histogram of the dust polarization's signal-to-noise ratio and AM between VGT and polarization.

5. Conclusion

Velocity gradients have demonstrated efficacy in tracing magnetic fields within MHD turbulence environments. This capability has been validated across various regions of the Milky Way and several Seyfert galaxies. In this paper, we extend the application of VGT to the more complex scenario of a merging galaxy. Specifically, we measure velocity gradients in the Centaurus galaxy and evaluate their effectiveness in tracing magnetic fields, using dust polarization as a comparative measure. Our findings indicate that VGT results generally concur with dust polarization on a statistical basis. Additionally, we identify localized regions of significant misalignment and antialignment. Drawing on prior studies, we hypothesize that outflows and the presence of shocked gas may account for these discrepancies. If corroborated, this comparison of gradients and polarization could elucidate the underlying physics of galactic mergers. Furthermore, our study aids in pinpointing regions within disturbed galaxies where velocity gradients can reliably map magnetic fields in the absence of other tracers. Future research, utilizing higher signal-to-noise

data and incorporating synchrotron polarization, is essential to further explore these findings.

Acknowledgments

A.L. acknowledges the support of NASA ATP AAH7546, NSF grants AST 2307840, and ALMA SOSPADA-016. Financial support for this work was provided by NASA through award 09_0231 issued by the Universities Space Research Association, Inc. (USRA). Y.H. acknowledges the support for this work provided by NASA through the NASA Hubble Fellowship grant No. HST-HF2-51557.001 awarded by the Space Telescope Science Institute, which is operated by the Association of Universities for Research in Astronomy, Incorporated, under NASA contract NAS5-26555. This work used SDSC Expanse CPU at SDSC through allocations PHY230032, PHY230033, PHY230091, and PHY230105 from the Advanced Cyberinfrastructure Coordination Ecosystem: Services & Support (ACCESS) program, which is supported by National Science Foundation grants #2138259, #2138286, #2138307, #2137603, and #2138296. Q.L.N. acknowledges the support in part by grant NSF PHY-1748958 to the Kavli Institute for Theoretical Physics (KITP), the Institute for Cosmic Ray Research-International University Research Program, Notre Dame College of Science Internal Grant.

Software: Julia (J. Bezanson et al. 2012).

ORCID iDs

Quynh Lan Nguyen https://orcid.org/0000-0002-1828-3702
Yue Hu https://orcid.org/0000-0002-8455-0805
Alex Lazarian https://orcid.org/0000-0002-7336-6674

References

Andersson, B. G., Lazarian, A., & Vaillancourt, J. E. 2015, ARA&A, 53, 501
Armstrong, J. W., Rickett, B. J., & Spangler, S. R. 1995, ApJ, 443, 209
Beck, R. 2001, SSRv, 99, 243
Beck, R. 2015, A&ARv, 24, 4
Bezanson, J., Karpinski, S., Shah, V. B., & Edelman, A. 2012, arXiv:1209.5145
Chepurnov, A., & Lazarian, A. 2010, ApJ, 710, 853
Chibueze, J. O., Sakemi, H., Ohmura, T., et al. 2021, Natur, 593, 47
Cho, J., & Lazarian, A. 2003, MNRAS, 345, 325
Cho, J., & Vishniac, E. T. 2000, ApJ, 539, 273
Duan, D., He, J., Bowen, T. A., et al. 2021, ApJL, 915, L8
Fletcher, A., Beck, R., Shukurov, A., Berkhuijsen, E. M., & Horellou, C. 2011, MNRAS, 412, 2396
Goldreich, P., & Sridhar, S. 1995, ApJ, 438, 763
González-Casanova, D. F., & Lazarian, A. 2017, ApJ, 835, 41
Ha, T., Li, Y., Kounkel, M., et al. 2022, ApJ, 934, 7
Harper, D. A., Runyan, M. C., Dowell, C. D., et al. 2018, JAI, 7, 1840008
Hu, Y., Lazarian, A., Alina, D., Pogosyan, D., & Ho, K. W. 2023, MNRAS, 524, 2994
Hu, Y., Lazarian, A., Beck, R., & Xu, S. 2022, ApJ, 941, 92
Hu, Y., Lazarian, A., & Bialy, S. 2020a, ApJ, 905, 129
Hu, Y., Lazarian, A., & Yuen, K. H. 2020b, ApJ, 897, 123
Hu, Y., Xu, S., & Lazarian, A. 2021, ApJ, 911, 37
Hu, Y., Yuen, K. H., & Lazarian, A. 2018, MNRAS, 480, 1333
Hu, Y., Yuen, K. H., & Lazarian, A. 2019, ApJ, 886, 17
Kandel, D., Lazarian, A., & Pogosyan, D. 2016, MNRAS, 461, 1227
Kowal, G., & Lazarian, A. 2010, ApJ, 720, 742
Kronberg, P. P. 1994, RPPh, 57, 325
Lazarian, A. 2006, ApJL, 645, L25
Lazarian, A., & Hoang, T. 2007, ApJ, 669, L77
Lazarian, A., & Pogosyan, D. 2000, ApJ, 537, 720
Lazarian, A., & Pogosyan, D. 2004, ApJ, 616, 943
Lazarian, A., & Vishniac, E. T. 1999, ApJ, 517, 700
Lazarian, A., & Yuen, K. H. 2018, ApJ, 853, 96
Leroy, A. K., Schinnerer, E., Hughes, A., et al. 2021, ApJS, 257, 43
Liu, M., Hu, Y., & Lazarian, A. 2024, MNRAS, 530, 1066
Liu, M., Hu, Y., Lazarian, A., Xu, S., & Soida, M. 2023, MNRAS, 519, 1068
Lopez-Rodriguez, E. 2021, NatAs, 5, 604
Maron, J., & Goldreich, P. 2001, ApJ, 554, 1175
Matteini, L., Franci, L., Alexandrova, O., et al. 2020, FrASS, 7, 83
Paliya, V. S., Pérez, E., García-Benito, R., et al. 2020, ApJ, 892, 133
Rodenbeck, K., & Schleicher, D. R. G. 2016, A&A, 593, A89
Struve, C., Oosterloo, T. A., Morganti, R., & Saripalli, L. 2010, A&A, 515, A67
Wang, X., Tu, C., Marsch, E., He, J., & Wang, L. 2016, ApJ, 816, 15
Whittingham, J., Sparre, M., Pfrommer, C., & Pakmor, R. 2021, MNRAS, 506, 229
Yuen, K. H., & Lazarian, A. 2017, ApJL, 837, L24
Zhao, M., Zhou, J., Baan, W. A., et al. 2024, ApJ, 967, 18
Zhao, S., Yan, H., Liu, T. Z., Yuen, K. H., & Shi, M. 2024, ApJ, 962, 89